# Large metabolic rewiring from small genomic changes between strains of *Shigella flexneri*

Sarah M. Doore[1*], Sundharraman Subramanian[1], Nicholas M. Tefft[1], Renato Morona[2], Michaela A. TerAvest[1#], and Kristin N. Parent[1#]

1. Department of Biochemistry and Molecular Biology, Michigan State University, East Lansing, MI 48824, USA
2. School of Molecular and Biomedical Science, University of Adelaide, 5005 SA, Australia

[*] Present address: Department of Microbiology and Cell Sciences, University of Florida, Gainesville, FL 32611, USA

[#]Co-Corresponding authors: teraves2@msu.edu and kparent@msu.edu

Running title: Metabolic rewiring of *S. flexneri* PE577

Key Words: *Shigella flexneri*, microaerobic metabolism, mixed acid fermentation, formate, acetate, acetyl-CoA

## Abstract

The instability of *Shigella* genomes has been described, but how this instability causes phenotypic differences within the *Shigella flexneri* species is largely unknown and likely variable. We describe herein the genome of *S. flexneri* strain PE577, originally a clinical isolate, which exhibits several phenotypic differences compared to the model strain 2457T. Like many previously described strains of *S. flexneri*, PE577 lacks discernible, functional CRISPR and restriction-modification systems. Its phenotypic differences when compared to 2457T include lower transformation efficiency, higher oxygen sensitivity, altered carbon metabolism, and greater susceptibility to a wide variety of lytic bacteriophage isolates. Since relatively few *Shigella* phages have been isolated on 2457T or the previously characterized strain M90T, developing a more universal model strain for isolating and studying *Shigella* phages is critical to understanding both phages and phage-host interactions. In addition to phage biology, the genome sequence of PE577 was used to generate and test hypotheses of how pseudogenes in this strain—whether interrupted by degraded prophages, transposases, frameshifts, or point mutations—have led to metabolic rewiring compared to the model strain 2457T. Results indicate that PE577 can utilise the less-efficient pyruvate oxidase/acetyl-CoA synthetase (PoxB/Acs) pathway to produce acetyl-CoA, while strain 2457T cannot due to a nonsense mutation in *acs*, rendering it a pseudogene in this strain. Both strains also utilize pyruvate-formate lyase to oxidize formate but cannot survive with this pathway alone, possibly because a component of the formate-hydrogen lyase (*fdhF*) is a pseudogene in both strains.

## Importance

*Shigella* causes millions of dysentery cases worldwide, primarily affecting children under five years old. Despite active research in developing vaccines and new antibiotics, relatively little is

known about the variation of physiology or metabolism across multiple isolates. In this work, we investigate two strains of *S. flexneri* that share 98.9% genetic identity but exhibit drastic differences in metabolism, ultimately affecting the growth of the two strains. Results suggest additional strains within the *S. flexneri* species utilize different metabolic pathways to process pyruvate. Metabolic differences between these closely-related isolates suggest an even wider variety of differences in growth across *S. flexneri* and *Shigella* in general. Exploring this variation further may assist the development or application of vaccines and therapeutics to combat *Shigella* infections.

## Introduction

*Shigella flexneri* is a causative agent of shigellosis, a type of bacillary dysentery. *Shigella* is endemic in numerous countries worldwide and contributes to the approximately 269.2 million cases of shigellosis per year (1). Dozens of *S. flexneri* serotypes and subtypes have been described, with each serotype determined by the lipopolysaccharide (LPS) O-antigen chemical structure (2, 3). These serotypes exhibit unique antigenic properties (4), and the genes responsible for determining serotype are often recombined and/or modified by lysogenic bacteriophages (3, 5), meaning serotype is a highly variable characteristic. Despite the large global burden of *S. flexneri* infections, relatively few strains have been thoroughly characterized; moreover, these strains represent an extremely small fraction of *S. flexneri* diversity (6). The model organism *S. flexneri* strain 2457T is serotype 2a—an antigenic type which is found worldwide—but belongs to only one of seven phylogenetic groups. Another commonly studied strain, *S. flexneri* M90T, is serotype 5a and belongs to a separate phylogenetic group with a narrower geographic range, primarily found in North America, Europe, and Southern Asia (6).

Besides these two strains, relatively little is known about other isolates or phylogenetic groups of the species.

PE577 is a serotype Y strain, with an O-antigen that is not decorated by glucosyl or acetyl moieties (3). This serotype serves as the most basic O-antigen structure, with other serotypes resulting from modification of the Y type. The strain was obtained from the Institute of Medical and Veterinary Science (now SA Pathology) in Adelaide, Australia in 1988. Though originally a clinical isolate, it has lost its virulence plasmid since isolation. Most recently isolated *S. flexneri*-infecting bacteriophages infect serotype Y, with some exclusively infecting this serotype (7, 8). A majority of these novel phages were isolated using strain PE577; comparably few were detected when non-pathogenic derivatives of other model strains 2457T or M90T were used, even from the same environmental samples. This strain has thus been useful for assessing both abundance and diversity of *Shigella* phages in the environment. While strain PE577 has been used to isolate and study many bacteriophages, it had not been previously described or characterized genomically or physiologically. Establishing a model organism with such widespread bacteriophage susceptibility may therefore advance our understanding of phage-host interactions, including O-antigen recognition and other determinants of host recognition. As part of this goal, we sequenced the entire genome of strain PE577, including its chromosome and two small plasmids. In addition, *Shigella* is known to produce variable responses in the human host (9, 10). Some of this is likely due to serotype and antigenicity, which has been the primary focus of vaccine development (4); however, some of the variability may also be due to variance in *Shigella* physiology and metabolism. Therefore, we also performed metabolic analyses of *S. flexneri* PE577 compared to CFS100, an avirulent derivative of 2457T (11), to measure

differences in carbon metabolism under aerobic or microaerobic conditions the bacteria may encounter while in the environment or moving through the human gut.

Unlike other genera of *Enterobacteriaceae*, *Shigella* lack functional CRISPR and restriction-modification systems and are susceptible to parasitism by mobile genetic elements (12). This likely contributes to the ongoing degradation of *Shigella* genomes, along with selective pressure to eliminate antivirulence genes, which interfere with the pathogenic lifestyle of these bacteria (13-15). While Connor et al. 2015 (6) describe overall stable genomes outside of these mobile elements, this work was based on large-scale whole genome sequencing data from hundreds of isolates: functional analyses were understandably beyond the scope of the study. In addition to its greater susceptibility to bacteriophage infection from samples collected from various environments (7, 8), we describe here that PE577 exhibits several differences in cell physiology compared to its 2a counterpart CFS100. These are exacerbated by microaerobic conditions and media where glucose is the primary carbon source compared to aerobic conditions and nutrient-rich media with a variety of carbon sources.

Through comparative genomics, we identified differences in genes involved in pyruvate catabolism between PE577 and CFS100. After determining the metabolic pathways in which these genes are involved, we examined the phenotypic effects of growing the two strains in a variety of conditions favored by alternate pathways. After growth, we measured specific metabolic products in spent media via HPLC to investigate which pathway(s) were utilized under each condition. The combination of genetic and metabolic analyses described herein indicate

that PE577 utilizes the PoxB/Acs bypass to generate acetyl-CoA while CFS100 does not. This metabolic rewiring suggests drastic physiological changes can occur from small genomic variation over a relatively short evolutionary history. These results have implications for *S. flexneri* pathogenesis, treatment, vaccine development, and bacteriophage susceptibility—including the research and development of phage therapy or its application.

## Results

### *PE577 belongs to a different* S. flexneri *phylogenetic group than other model strains*

To begin comparing genetic changes between strains, the complete genome of *S. flexneri* strain PE577 was sequenced, including its 4.6 Mbp chromosome and two plasmids (Figure 1). Individual characteristics and accession numbers of these are shown in Table 1, which can be cross-referenced using the accession numbers PRJNA533747 for BioProject or SAMN12588114 for BioSample.

Previous work has consolidated worldwide *S. flexneri* isolates into seven phylogenetic groups (PGs), which cluster by location and serotype (refer to Figure 1 and supplementary material contained within Conner et al. (6)). Strains of serotype Y are primarily found in four of these groups: PG1, PG3, PG6, and PG7. These PGs can be further distinguished by the presence of serine protease autotransporter toxin genes *sigA*/*sat* and *pic*, the iron uptake *sit* and *fec* operons, the enterobactin *ent* operon, and the *Shigella* enterotoxin 1 (ShET1) genes *set1A* and *set1B*. Strain PE577 encodes all but the Fec operon and ShET1 genes. Combined, these characteristics suggest that PE577 is a member of PG7, which is predominantly found in east and southeast

134 Asia—consistent with PE577 originating in Australia. By contrast, the phylogenetic groups of
135 2457T and M90T are PG3 and PG5, respectively. Strains of PG3 were isolated from around the
136 world, while PG5 is primarily composed of historical strains originating from North America and
137 Europe. Strain PE577 therefore provides a third representative for comparing separate
138 phylogenetic and geographic groups within the species. Since PE577 is the host to numerous
139 bacteriophages, an analysis of prophage remnants was conducted using the PHAge Search Tool –
140 Enhanced Released (PHASTER) search tool (16). Genome remnants from at least eleven phages
141 are present, and include identity to known phages such as iGifsy-1, Sf6, sal3, Stx2, N4, etc.
142 Additionally, this region includes some structural genes of unknown origin. While the full
143 genomes of these phages are incomplete, some genes remain intact. These are primarily limited
144 to transposases, though some regions also include structural phage genes. These prophages are
145 indeed defunct as no phage particles were produced after induction (data not shown).

146

147 In addition to the chromosome, PE577 harbors two plasmids, characterized by similarities to
148 ColE1 and pHS-2 (17, 18). The first of these encodes seven full-length proteins, including
149 mobilization proteins in the *mob/mbe* operon. This plasmid has been found in numerous strains
150 of enteric bacteria, where it frequently encodes additional transposable elements or antibiotic
151 resistance genes (17). Thus far, at least among strains of *S. flexneri*, only the mobilization operon
152 is present, suggesting the additional genes are either not retained or have not yet been
153 transferred. Since this plasmid encodes the full-length exclusion protein MbeD, transferring a
154 similar *mob/mbe* operon-encoding plasmid is unlikely. The second plasmid resembles the stably
155 maintained pHS-2, which has been found in many *Shigella* and *E. coli* isolates (19). It encodes
156 two small full-length proteins, along with $Wzz_{pPHS2}$, a regulator of lipopolysaccharide O-antigen

157 length (20, 21). The chromosomally encoded allele of *fepE* contains an internal stop codon, but
158 the plasmid encodes a full-length homolog. This has been seen in other strains of *S. flexneri*,
159 including 2457T (22, 23).

160

161 The chromosomes of PE577 and 2457T exhibit 98.9% average nucleotide identity, calculated as
162 the query coverage multiplied by percent identity, with only one large ~1 mega base inversion.
163 Compared to the alternate model strain M90T, PE577 shares an average nucleotide identity of
164 96.9%, with several rearrangements throughout the genome. Despite this overall close similarity,
165 PE577 and CFS100 are distinct during routine laboratory growth: PE577 cultures contain fewer
166 colony forming units (CFU) per mL after overnight growth, and they grow poorly in
167 microaerobic conditions or in minimal media (Figure 2). Combined, these qualities suggest
168 systematic differences between these two strains, which may contribute to PE577's enhanced
169 susceptibility to bacteriophages. To measure these differences more quantitatively, specific
170 properties were investigated in greater detail.

171

172 *PE577 exhibits metabolic differences compared to model strain 2457T*

173 To characterize PE577, general properties were first determined and compared to CFS100, an
174 established model organism. CFS100 is an avirulent derivative of the model organism *S. flexneri*
175 2457T (11). First, overnight cell densities were measured in nutrient-rich or minimal media, and
176 in aerobic or microaerobic conditions. Different levels of aeration were achieved by growing
177 cultures in tubes with: 1) loose caps and over 5x volume of headspace for good aeration, versus
178 2) tubes with screw caps and less than 1/5 volume of headspace for poor aeration

179 ("microaerobic" conditions). Based on colony forming units (CFU) per mL, PE577 grew to
180 slightly lower density than CFS100 in nutrient-rich conditions, with the greatest decrease in
181 microaerobic conditions (data not shown). In minimal media, PE577 growth was significantly
182 lower than CFS100 in both aerobic and microaerobic conditions. To further investigate the effect
183 of nutrients on growth between these two strains, growth curves were conducted for 6 hr under
184 aerobic conditions, with measurements taken as colony forming units (CFU) per mL and optical
185 density at 600nm (OD600). As shown in Figure 2A, PE577 grows significantly slower than
186 CFS100 in terms of CFU/mL in both types of media, with hardly any growth in M9 minimal
187 media. In addition, while both strains showed initial lower OD600 readings in minimal media,
188 CFS100 ultimately returned to densities similar to growth in nutrient-rich media (Figure 2B).
189 Conversely, PE577 density increased slightly over time but never reached levels of LB growth.
190 Despite this, there was no clear change in the relationship between OD600 and CFU/mL for
191 PE577 based on media type (Figure 2C). When the dimensions of individual cells from each
192 strain were measured after overnight growth in LB or M9, PE577 was elongated compared to
193 CFS100, though both cell types were longer in M9 than in LB (Supplementary Table 1,
194 Supplementary Figure 1).

195

196 To examine potential changes in physiology between these two strains in minimal media,
197 residual glucose was measured in media after overnight growth. Up to 36.7% of the initial
198 glucose was unused in PE577 cultures (2.94 ± 2.43 mM remaining of 12.87 mM starting
199 glucose). While highly variable, this was contrasted by the residual glucose composition of spent
200 CFS100 media, which was consistently below the limit of detection after overnight growth.
201 These results suggested an inefficiency or inconsistency in PE577 glucose catabolism under

202 microaerobic conditions. To develop this hypothesis further, we specifically examined genes
203 involved in glycolysis and fermentation. We created a comprehensive list of all pseudogenes
204 found in PE577 (Supplementary Table 2) and CFS100 (Supplementary Table 3), then analyzed
205 them to see which pseudogenes were unique to each strain (Table 2).

206

207 From a comparison to the CFS100 parental 2457T genome (22), PE577 was found to encode a
208 frameshifted, truncated version of HycC, which is a subunit of the formate hydrogenlyase
209 complex (FHL, Figure 3A; (24)). A 16-nucleotide insertion in the PE577 *hycC* gene results in a
210 frameshift, causing a premature stop codon: the new coding sequence is for a 298-amino acid
211 protein rather than the 597 amino acid HycC protein in CFS100 (Figure 3B). The FHL complex
212 is responsible for oxidizing formate produced by pyruvate-formate lyase (PFL), which converts
213 pyruvate to formate and acetyl-coA(24, 25). While the better-characterized strains of *S. flexneri*
214 encode full-length HycC, protein databases indicate that numerous other strains of *S. flexneri*
215 encode truncated versions of HycC: for example, in a BLAST query using the PE577 protein
216 sequence, 42 out of 89 *S. flexneri*-specific hits were similarly truncated at a range between 274
217 and 325 amino acids. While a complete *hycC* deletion mutant still exhibits functional FHL
218 activity *in vitro* (25), the complex is unable to transport resulting protons out of the cell *in vivo*,
219 resulting in an overall decreased rate of formate oxidation (26). From an analysis of single amino
220 acid substitutions throughout the protein, only two changes, D354A and E391A, significantly
221 reduced formate-dependent hydrogen production (26). The effect of a truncated version—where
222 HycC lacks six C-terminal transmembrane helices of thirteen total—has not been described.

223

Since the HycC truncation in strain PE577 includes the region identified by Pinske and Sargent as important for FHL activity *in vivo* (26), we hypothesized that this strain would be unable to convert formate to carbon dioxide and hydrogen as effectively as CFS100. To test whether PE577 media contains greater levels of formate when compared to CFS100, single colonies of PE577 or CFS100 were grown in minimal media where glucose was the primary carbon source, and in conditions where oxygen was limited. After overnight incubation, the cells were then removed by centrifugation and fermentation products in the supernatant were measured by HPLC. As shown in Figure 4D, these measurements indicate that strain PE577 produces *less* formate than CFS100, with an average of 6.06 ± 1.34 mM formate for PE577 and 11.41 ± 0.35 mM formate for CFS100. These results nullified the hypothesis that the truncated HycC results in a buildup of formate, but the greater variation in formate production between biological replicates of PE577 suggests there may be some other effect. An additional confounding factor is that in *E. coli*, the canonical formate dehydrogenase associated with FHL is encoded by *fdhF* (26); however, this is a pseudogene in both *S. flexneri* strains PE577 and 2457T (Figure 3), encoding only 79 amino acids. Whether *Shigella* can use a different formate dehydrogenase in conjunction with FHL or uses HycC in a different pathway or complex is unclear.

*PE577 and CFS100 use different mechanisms to generate acetyl-CoA in microaerobic conditions*

The variation in PE577 formate accumulation could be explained by two mechanisms: 1) the truncated HycC protein functions enough to allow the FHL complex to remain active, albeit at variable levels; or 2) PE577 produces variable levels of formate, providing more flexibility to bypass the requirement for FHL activity. To investigate these possibilities, *hycC* was completely deleted in both strains and the resulting knockouts were characterized. The PE577*ΔhycC* was

247 indistinguishable from the parental PE577 strain in terms of CFU/mL and fermentation products
248 (Figure 4), whereas the CFS100*ΔhycC* mutant exhibited a severe growth defect and an altered
249 fermentation profile relative to both wild-type strains. Complementing CFS100*ΔhycC* with either
250 the truncated PE577 or full-length CFS100 *hycC* gene restored both the growth and metabolite
251 profile of this strain (Figure 4). These results suggest that: 1) FHL is functional, despite the *fdhF*
252 pseudogene; 2) CFS100 relies on FHL in microaerobic conditions; and 3) PE577—despite
253 having a functional HycC—does not require this pathway. Since overnight growth and metabolic
254 products were not significantly different from each other, a measurable difference in HycC
255 activity between the full-length and truncated versions seems unlikely.

256

257 As an alternative to PFL, pyruvate can be oxidized directly to acetyl-CoA in by pyruvate
258 dehydrogenase (PDH) or indirectly through an acetate intermediate via the ubiquinone-
259 dependent pyruvate oxidase (PoxB). Acetate is then ligated to coenzyme A by acetate-CoA
260 synthetase (Acs) to produce acetyl-CoA in an anaerobic PoxB/Acs bypass (Figure 3A; (27, 28)).
261 Although PoxB expression is highest under aerobic conditions, it is still active in low oxygen
262 conditions (29). Generally, the PoxB/Acs bypass is regarded as less efficient than the PFL/FHL
263 pathway during exponential growth and is instead only used to mediate the transition between
264 exponential and stationary phases or during periods of slow growth (27, 29). Relying on this
265 mechanism to produce acetyl-CoA avoids the production of formate and could explain some of
266 the variation in PE577 formate accumulation.

267

268 An examination of the CFS100 genome revealed the *acs* gene encodes a truncated protein of 248
269 amino acids, compared to the 652 amino acid protein in PE577 (Figure 3B). Based on protein
270 database entries, truncated or partial Acs proteins are also found in other *S. flexneri* strains (10 of
271 the top 37 high scoring alignments), including numerous reference sequences. In addition,
272 CFS100 also encodes a truncated RpoS protein, predicted to lack the HTH motif. Since *poxB*
273 transcription is mediated by RpoS, this may affect overall levels of PoxB.

274

275 To further explore pyruvate metabolism in both strains, we generated deletions of PFL (*pflB*),
276 PDH (*aceE*), and the PoxB/Acs bypass and analyzed them in the same way as the HycC deletion
277 strains (Figure 5). We observed that both strains showed very similar phenotypes when *pflB* was
278 deleted, with little impact on growth but the abolition of formate production, an increase in
279 lactate production, and a decrease in acetate production. This suggests that both strains utilize
280 PFL to oxidize pyruvate, but the activity is dispensable. Conversely, an *aceE* deletion produced
281 drastically different phenotypes between the two strains, with only a small growth defect in
282 PE577 compared to a greater than 4-log reduction in final cell density for CFS100. This is
283 consistent with the lack of a functional *acs* in CFS100: PE577 has an additional route for
284 pyruvate oxidation, making the *aceE* deletion less harmful, whereas CFS100 has no effective
285 alternative. The *poxB* and *acs* deletions did not cause strong phenotypes in either strain,
286 consistent with previous literature suggesting that this route plays a minor role in pyruvate
287 oxidation under normal circumstances.

288

289 **Discussion**

290 *Altered carbon flux from few genetic changes*

291 Despite the close genetic identity between the two strains PE577 and CFS100, they exhibit
292 significantly different phenotypes in terms of growth, morphology, and metabolism. Although
293 these strains are distinct isolates and are therefore not isogenic, assigning specific genetic
294 changes to phenotypic changes is difficult; however the differences can nevertheless be
295 informative. Based on our results, it appears that while PE577 and CFS100 primarily rely on
296 PFL to convert pyruvate to acetyl-CoA in micro- or anaerobic conditions, PE577 is also capable
297 of using the PoxB/Acs bypass to generate acetyl-CoA. Since this latter pathway is active under a
298 different set of growth conditions and is overall a minor contributor to pyruvate oxidation, this
299 could explain some of the variation observed in PE577 formate production. It is unclear how this
300 rewiring evolved, and whether the truncated HycC of the FHL complex arose before or after this
301 switch.

302

303 Inefficient acetyl-CoA production by the PoxB/Acs bypass could also explain morphological
304 differences between these two strains. For example, modest defects in cell division could explain
305 the elongated phenotype of PE577 compared to CFS100, with this defect exacerbated under
306 nutrient-limited conditions (30). In addition, as a critical component of fatty acid synthesis,
307 reduced acetyl-CoA availability could limit the amount or the type of phospholipids available for
308 the membrane. PE577 cells display “pointed” poles (see Supplementary Figure 1), which have
309 been seen in *E. coli* cells lacking the phosphatidylethanolamine (PE) biosynthetic pathway (31).
310 As a major component of the membrane, PE-deficient cells exhibit clear structural defects
311 compared to wild-type cells, including increased production of outer membrane vesicles and
312 detachment of the inner membrane from the outer membrane. These cells also show severely

313 delayed growth in M9 media, only entering exponential phase around 3 h (31), which is the same
314 delay as PE577. Alternatively, additional changes in the genome could explain the altered
315 morphology. For example, *mreC* encodes a rod shape-determining protein, and knockdowns
316 have been shown to affect cell size and shape (32). The CFS100 genome encodes a truncated
317 version of this protein (Table 2), which could lead to an overall rounder shape.

318

319 *Implications for persistence and virulence*

320 Using 2457T, the parental strain of CFS100, it has been shown that formate induces expression
321 of virulence genes *icsA* and *ipaJ*, both of which are encoded on the 200 kbp virulence plasmid
322 (33). These gene products control cell-to-cell spread and modulate the host immune response,
323 respectively (34-37). A mutant *ΔpflB* strain exhibits attenuated intracellular growth and
324 intercellular movement, suggesting that *S. flexneri*-produced formate induces efficient expression
325 of virulence genes (33). Exogenously applied formate can also induce genes, suggesting formate
326 metabolism itself is not required for virulence; rather, when *S. flexneri* produces formate and
327 releases it into the cell, it is the local increase in formate concentration that induces expression of
328 virulence genes. Conversely, exogenously applied acetate has no apparent effect on virulence
329 (33). In the intracellular environment, where pyruvate is readily accessible, *S. flexneri* has been
330 shown to use the quicker pyruvate-to-acetate pathway, producing large amounts of acetate to
331 facilitate rapid growth (38). Of note, these experiments were done using strain 2457T, which
332 lacks acetyl-CoA synthetase and is therefore unable to convert acetate into acetyl-CoA.

333

Since strain PE577 appears to have an additional route to bypass formate production, other virulent strains with similar genome signatures—a truncated HycC and the presence of acetyl-CoA synthetase—may have similar metabolic rewiring. It is unclear whether a *ΔpflB* mutant in these backgrounds would affect virulence similar to 2457T. Formate and acetate are known to influence pathogenicity of small intestine pathogens such as *Salmonella enterica* sv. Typhimurium (39, 40) and enteropathogenic *E. coli* (41). In *S. enterica* sv. Typhimurium, either acetate or formate can induce the expression of invasion genes (39, 40), while acetate is the primary signal for enteropathogenic *E. coli* adhesion and motility (41). In *S. flexneri*, there may be intraspecies variation for virulence gene induction, with some strains relying on formate and others relying on acetate, perhaps through the induction of different sets of virulence genes.

This may suggest that a group of closely related *Shigella* strains, with a range of genetic adaptations or in various stages of evolution, lead to the observed variations in virulence. These physiological changes may facilitate bacteriophage infection, often leading to phage-mediated serotype conversion, further contributing to the genetic pool from which human-adapted virulence strains arise.

*Establishing a model serotype Y strain*

In this work, we investigated genomic, physiological, and metabolic differences between strain PE577 and another model strain of *S. flexneri*, CFS100. The PE577 strain has been instrumental for analyzing abundance and diversity of phages from the environment, in addition to characterizing numerous phages. While two model strains have already been described for *S.*

*flexneri*, the variability between isolates warrants further study. We describe here significant differences between the physiology and metabolism of PE577 and CFS100 (avirulent 2457T), but it is unclear how widespread these differences are and whether these differences affect *S. flexneri* persistence in the environment or its virulence.

## Materials and Methods

### *Strains, plasmids, and media*

*S. flexneri* strain PE577 was a gift from R. Morona at University of Adelaide. It was originally obtained from C. Murray at the Institute of Medical and Veterinary Science in South Australia by P. Manning at the University of Adelaide in December 1988. Strain CFS100 was a gift from I. Molineux at the University of Texas—Austin and has been described (11).

For PCR amplification, mutagenesis and cloning, plasmids pKD4 (AddGene #45605) or pKD13 were used as templates for amplifying kanamycin cassettes; pKM208 (AddGene #13077) was used for recombination; and pGRB (AddGene #71539) was used for cloning. These plasmids have been previously described (42-44). To clone into pGRB, the gene of interest was amplified by PCR using primers that introduced homologous regions of the multi-cloning site. To linearize the plasmid, pGRB was digested with EcoRI and HindIII. The plasmid and PCR product were added to Gibson Assembly master mix according to the manufacturer's protocol. After assembly, the product was transformed and colonies were recovered. The insert size was determined by agarose gel electrophoresis and the sequence confirmed by Sanger sequencing.

377

378 Minimal media was comprised of 0.1 mM $CaCl_2$, M9 salts, 0.2% glucose, 1 mM MgSO4, and
379 supplemented with amino acids (0.2 mM histidine, 0.6 mM leucine, 0.3 mM methionine, 0.1 mM
380 tryptophan), 0.3 μM thiamine HCl and 0.1 mM niacin.

381

382 *Growth Curves and Microscopy*

383 Growth curves were conducted under aerobic conditions, using 25 mL media in Erlenmeyer
384 flasks while shaking. Media was inoculated using 2% v/v of an overnight culture grown in the
385 same media. Every 30 min, cell density was determined by optical density at 600 nm and an
386 aliquot was taken to determine CFU/mL. These experiments were conducted three times. To
387 measure cell dimensions, 1 mL overnight cultures were centrifuged to concentrate cells and
388 resuspended in 50 μL buffer (10mM $MgCl_2$, 10mM Tris pH 7.6) or water for cryo-electron
389 microscopy. Small aliquots (~5 μL) were then applied to R2/2 Quantifoil grids that had been
390 glow discharged for 60 s in a Pelco EasyGlow discharge unit. Samples were plunge frozen into
391 liquid ethane using a Vitrobot Mark IV under 100% humidity at 4°C with a blot force of 1 and
392 blot time of 4 s. Cells were viewed in an FEI Talos Arctica, with micrographs collected on a Ceta
393 camera at 11,000 X nominal magnification (9.66 Å/pixel). Individual cells' dimensions were
394 measured using ImageJ and Adobe Photoshop.

395

396 *DNA Extraction and Sequencing Methods*

Chromosomal DNA was extracted from 5 mL of *S. flexneri* PE577 overnight culture using a standard phenol/chloroform protocol, followed by ethanol precipitation with the addition of 0.3M sodium acetate. Purity was determined by measuring absorbance at 230, 260, and 280 nm. Plasmid DNA was extracted from 50 mL of overnight culture using the ZymoPure II Plasmid Midi Kit, with individual plasmids purified via gel electrophoresis. These were then subsequently extracted via Zymoclean Gel or Large Fragment DNA Recovery Kits.

Separate sequencing technologies were used for the chromosome and two small plasmids. Strain PE577 strain lacks the 200 kbp virulence plasmid pWR100, which was verified by PCR using primers that target the *virG* (F: 5'-TTA TGG TGA GGG TGA TGG CG-3'; R: 5'-GGG ATT TTC CGT CCC AGC TA-3') and *virB* (F: 5'-CCG GGG GCA GAT TTG TAT CA-3'; R: 5'-TGG TGG ATT TGT GCA ACG AC-3') genes. Strain M90T, which contains pWR100, was used as a positive control. In addition, total plasmid isolated from 100 mL of overnight culture using a ZymoPURE II Plasmid Midiprep Kit revealed only two small plasmids based on agarose gels and sequencing. The chromosome was sequenced using 250 bp paired-end reads on an Illumina HiSeq at MicrobesNG, with a minimal coverage of 30x. These were then assembled into a single 4.6 Mbp contig using the A5 pipeline, version 08-25-2016 (45). The plasmids were sequenced at the Massachusetts General Hospital Center for Computational and Integrative Biology (MGH CCIB) DNA Core, where they were assembled into 4.0 kbp, and 3.1 kbp contigs. The minimal coverage for each plasmid was 3150x and 2015x, respectively. Since all molecules are circular, the termini are based on reference sequences. Sequences were then annotated via the NCBI Prokaryotic Genome Annotation pipeline and submitted to GenBank (accession numbers CP042978.1 and CP042979.1 for plasmids, CP042980.1 for the chromosome).

420

421 *Generation of mutants*

422 Competent PE577 and CFS100 cells harboring the pKM208 plasmid were generated by
423 inoculating 100 mL of LB with 2 mL of overnight culture. Cells were grown with 4 mM IPTG
424 and 100 µg/mL ampicillin at 27.5° C to an $OD_{600}$ of ~ 0.4 and pelleted by centrifugation of 1,500
425 x g for 10 minutes at 4°C. The cells were resuspended in ice-cold water, centrifuged again at
426 1,500 x g for 10 minutes at 4°C. This pellet was gently resuspended in 5 mL of ST buffer (0.125
427 % Yeast Extract, 0.25 % Tryptone, 10 % PEG8000, 7% DMSO) by swirling. The cells were
428 subsequently pelleted by centrifuging at 1,500 x g for 15 minutes at 4°C, followed by a final
429 resuspension in 2 mL of ST buffer by swirling. 100 µL aliquots of cells were used for each
430 transformation reaction.

431

432 PCR products containing the kanamycin cassette for recombination were generated by designing
433 primers for two schemes. In the first, primers bind ~500bp upstream and downstream of the gene
434 of interest (e.g. for *hycC*, LH1: 5' GCG CGG CGA GAT AAT GTT GAC CTA ATT TTT CTT
435 CAG ACA TGC TCA AAC 3'; LH2: 5' GGC GTG TCG ATG AGT GTC GAA AAT GAC
436 ATT TCA TCG GCA TGT TTT CG 3'). In the second scheme, one set of primers binds to either
437 end of the antibiotic resistant cassette of pKD4 or pKD13 with ~20 additional nucleotides
438 matching the gene of interest (e.g. for *hycC*, Rxn1F: 5' GGT TTG TCG CCG CCG CTG TTC
439 TGT GTA GGC TGG AGC TGC TTC GAA GTT C 3'; Rxn1R: 5' CCA CCA GTA CCG CCA
440 GTT CAA CCA GCG CAA TTC CGG GGA TCC GTC GAC C 3'); the second set of primers
441 matches the gene of interest, with ~15 bp overlapping sequence between the two sets of primers

(Rxn2F: 5' GCA ATT TCC CTG ATC AAT AGC GGC GTG GCA TGG TTT GTC GCC GCC GCT G 3'; Rxn2R: 5' CAC TCA TTC TCA GGC TCC TCG TGA AAC AAT AAT CAC CAC CAG TAC CGC CAG TT 3' ). After the second reaction, 10 µL of final product was added to 100 µL of competent cells and gently mixed by pipetting up and down, followed by incubation in ice for 5 min. After electroporation with a Bio-Rad Gene Pulser Xcell system, using a current of 2.5kV in 0.2cm cuvettes, cells were recovered in 1 mL of SOC media at 30° C for 90 minutes. Mutant clones were then confirmed by colony PCR with primers that bind upstream, and downstream of the gene of interest (LH1 and LH2).

*Analysis of mixed acid fermentation products*

Minimal media was inoculated with a single colony for each replicate, with three replicates per set. For aerobic conditions, cultures were grown in standard culture tubes with loose caps; for microaerobic conditions, screw-cap culture tubes were used with minimal headspace (< 1 mL volume for 5 mL of culture). When stricter anaerobic conditions or alternative media were used, PE577 was unable to grow to measurable optical density or CFU/mL. Tubes were placed in a rotating wheel overnight. An aliquot of each culture was used to measure cell concentrations by colony counts. Cultures were then spun for 10 min at 8,000 x g to remove cells, then supernatants were transferred to 2 mL glass HPLC tubes.

HPLC analysis was conducted as described in (46). Briefly, compounds of interest were separated using a 0.6 mL/min flow rate in 5 mM sulfuric acid with a 30 min run time. The eluent was prepared by diluting a 50% HPLC-grade sulfuric acid solution (Fluka) in Milli-Q water and

degassing the solution at 37 °C for 3–5 days before use. Compounds of interest were detected by a refractive index detector (Shimadzu, RID-20A) maintained at 50°C, using an Aminex HPX-87H column with a Micro Guard cation H+ guard (Bio Rad, Hercules, CA). Mixed standards were prepared for glucose, acetate, formate, and lactate at concentrations of 0.5, 0.75, 1, 2, 3, 5, and 10 mM. Standards and samples were maintained at 10 °C by an autosampler (Shimadzu, SIL-20AHT) throughout the analysis.

**Acknowledgements**

The authors would like to thank Dr. Ian Molineux for providing strains of bacteria and for helpful discussions, and Dr. Sherwood Casjens for helpful discussions. We also thank John Dover, Tori Brown, Ashleigh Bass, and Vanessa Eaton for optimizing M9 composition and initial growth characterization; and the MSU RTSF Cryo-EM Facility for preparation and imaging of cells. This work was funded by the National Institutes of Health GM110185, the National Science Foundation CAREER Award 1750125, the JK Billman Jr, MD Endowed Research Professorship, and Burroughs Wellcome Fund Award to KNP; the National Science Foundation CAREER Award 1750785 and a Beckman Young Investigator award from the Arnold and Mabel Beckman Foundation to MT; and the Australian Reseach Council Discovery Project DP170104325 to RM. Any opinions, findings, and conclusions or recommendations expressed in this material are those of the author(s) and do not necessarily reflect the views of the funders.

## References


1. **Collaborators GBDDD.** 2018. Estimates of the global, regional, and national morbidity, mortality, and aetiologies of diarrhoea in 195 countries: a systematic analysis for the Global Burden of Disease Study 2016. Lancet Infect Dis **18:**1211-1228.
2. **Sethuvel DPM, Ragupathi NKD, Anandan S, Veeraraghavan B.** 2017. Update on: Shigella new serogroups/serotypes and their antimicrobial resistance. Letters in Applied Microbiology **64:**8-18.
3. **Knirel YA, Sun Q, Senchenkova SN, Perepelov AV, Shashkov AS, Xu J.** 2015. O-antigen modifications providing antigenic diversity of Shigella flexneri and underlying genetic mechanisms. Biochemistry (Mosc) **80:**901-914.
4. **Livio S, Strockbine NA, Panchalingam S, Tennant SM, Barry EM, Marohn ME, Antonio M, Hossain A, Mandomando I, Ochieng JB, Oundo JO, Qureshi S, Ramamurthy T, Tamboura B, Adegbola RA, Hossain MJ, Saha D, Sen S, Faruque AS, Alonso PL, Breiman RF, Zaidi AK, Sur D, Sow SO, Berkeley LY, O'Reilly CE, Mintz ED, Biswas K, Cohen D, Farag TH, Nasrin D, Wu Y, Blackwelder WC, Kotloff KL, Nataro JP, Levine MM.** 2014. Shigella isolates from the global enteric multicenter study inform vaccine development. Clin Infect Dis **59:**933-941.
5. **Allison GE, Verma NK.** 2000. Serotype-converting bacteriophages and O-antigen modification in Shigella flexneri. Trends Microbiol **8:**17-23.
6. **Connor TR, Barker CR, Baker KS, Weill FX, Talukder KA, Smith AM, Baker S, Gouali M, Pham Thanh D, Jahan Azmi I, Dias da Silveira W, Semmler T, Wieler LH, Jenkins C, Cravioto A, Faruque SM, Parkhill J, Wook Kim D, Keddy KH, Thomson NR.** 2015. Species-wide whole genome sequencing reveals historical global spread and recent local persistence in Shigella flexneri. Elife **4:**e07335.
7. **Doore SM, Schrad JR, Dean WF, Dover JA, Parent KN.** 2018. Shigella Phages Isolated during a Dysentery Outbreak Reveal Uncommon Structures and Broad Species Diversity. Journal of Virology **92**.
8. **Doore SM, Schrad JR, Perrett HR, Schrad KP, Dean WF, Parent KN.** 2019. A cornucopia of Shigella phages from the Cornhusker State. Virology **538:**45-52.
9. **Islam MM, Azad AK, Bardhan PK, Raqib R, Islam D.** 1994. Pathology of shigellosis and its complications. Histopathology **24:**65-71.
10. **Zaidi MB, Estrada-Garcia T.** 2014. Shigella: A Highly Virulent and Elusive Pathogen. Curr Trop Med Rep **1:**81-87.
11. **Marman HE, Mey AR, Payne SM.** 2014. Elongation factor P and modifying enzyme PoxA are necessary for virulence of Shigella flexneri. Infect Immun **82:**3612-3621.
12. **Subramanian S, Parent KN, Doore SM.** 2020. Ecology, Structure, and Evolution of Shigella Phages. Annu Rev Virol doi:10.1146/annurev-virology-010320-052547.
13. **Maurelli AT.** 2007. Black holes, antivirulence genes, and gene inactivation in the evolution of bacterial pathogens. FEMS Microbiol Lett **267:**1-8.
14. **Maurelli AT, Fernandez RE, Bloch CA, Rode CK, Fasano A.** 1998. "Black holes" and bacterial pathogenicity: a large genomic deletion that enhances the virulence of Shigella spp. and enteroinvasive Escherichia coli. Proc Natl Acad Sci U S A **95:**3943-3948.
15. **Bliven KA, Maurelli AT.** 2012. Antivirulence genes: insights into pathogen evolution through gene loss. Infect Immun **80:**4061-4070.
16. **Arndt D, Grant JR, Marcu A, Sajed T, Pon A, Liang Y, Wishart DS.** 2016. PHASTER: a better, faster version of the PHAST phage search tool. Nucleic Acids Res **44:**W16-21.
17. **Ares-Arroyo M, Bernabe-Balas C, Santos-Lopez A, Baquero MR, Prasad KN, Cid D, Martin-Espada C, San Millan A, Gonzalez-Zorn B.** 2018. PCR-Based Analysis of ColE1 Plasmids in Clinical

Isolates and Metagenomic Samples Reveals Their Importance as Gene Capture Platforms. Front Microbiol **9:**469.

18. **Rehel N, Szatmari G.** 1996. Characterization of the stable maintenance of the Shigella flexneri plasmid pHS-2. Plasmid **36:**183-190.
19. **Adam T, Siewerdt R, Offermann I, Lang J, Tschape H, Sieper J, Graf B.** 2003. Prevalence and molecular diversity of pHS-2 plasmids, marker for arthritogenicity, among clinical Escherichia coli Shigella isolates. Microbes Infect **5:**579-592.
20. **Purins L, Van Den Bosch L, Richardson V, Morona R.** 2008. Coiled-coil regions play a role in the function of the Shigella flexneri O-antigen chain length regulator WzzpHS2. Microbiology **154:**1104-1116.
21. **Morona R, Purins L, Tocilj A, Matte A, Cygler M.** 2009. Sequence-structure relationships in polysaccharide co-polymerase (PCP) proteins. Trends Biochem Sci **34:**78-84.
22. **Wei J, Goldberg MB, Burland V, Venkatesan MM, Deng W, Fournier G, Mayhew GF, Plunkett G, 3rd, Rose DJ, Darling A, Mau B, Perna NT, Payne SM, Runyen-Janecky LJ, Zhou S, Schwartz DC, Blattner FR.** 2003. Complete genome sequence and comparative genomics of Shigella flexneri serotype 2a strain 2457T. Infect Immun **71:**2775-2786.
23. **Hong M, Payne SM.** 1997. Effect of mutations in Shigella flexneri chromosomal and plasmid-encoded lipopolysaccharide genes on invasion and serum resistance. Mol Microbiol **24:**779-791.
24. **Sauter M, Bohm R, Bock A.** 1992. Mutational analysis of the operon (hyc) determining hydrogenase 3 formation in Escherichia coli. Mol Microbiol **6:**1523-1532.
25. **McDowall JS, Murphy BJ, Haumann M, Palmer T, Armstrong FA, Sargent F.** 2014. Bacterial formate hydrogenlyase complex. Proc Natl Acad Sci U S A **111:**E3948-3956.
26. **Pinske C, Sargent F.** 2016. Exploring the directionality of Escherichia coli formate hydrogenlyase: a membrane-bound enzyme capable of fixing carbon dioxide to organic acid. Microbiologyopen **5:**721-737.
27. **Abdel-Hamid AM, Attwood MM, Guest JR.** 2001. Pyruvate oxidase contributes to the aerobic growth efficiency of Escherichia coli. Microbiology **147:**1483-1498.
28. **Wolfe AJ.** 2005. The acetate switch. Microbiol Mol Biol Rev **69:**12-50.
29. **Chang YY, Wang AY, Cronan JE, Jr.** 1994. Expression of Escherichia coli pyruvate oxidase (PoxB) depends on the sigma factor encoded by the rpoS(katF) gene. Mol Microbiol **11:**1019-1028.
30. **Westfall CS, Levin PA.** 2018. Comprehensive analysis of central carbon metabolism illuminates connections between nutrient availability, growth rate, and cell morphology in Escherichia coli. PLoS Genet **14:**e1007205.
31. **Rowlett VW, Mallampalli V, Karlstaedt A, Dowhan W, Taegtmeyer H, Margolin W, Vitrac H.** 2017. Impact of Membrane Phospholipid Alterations in Escherichia coli on Cellular Function and Bacterial Stress Adaptation. J Bacteriol **199**.
32. **Kruse T, Bork-Jensen J, Gerdes K.** 2005. The morphogenetic MreBCD proteins of Escherichia coli form an essential membrane-bound complex. Mol Microbiol **55:**78-89.
33. **Koestler BJ, Fisher CR, Payne SM.** 2018. Formate Promotes Shigella Intercellular Spread and Virulence Gene Expression. mBio **9**.
34. **Bernardini ML, Mounier J, d'Hauteville H, Coquis-Rondon M, Sansonetti PJ.** 1989. Identification of icsA, a plasmid locus of Shigella flexneri that governs bacterial intra- and intercellular spread through interaction with F-actin. Proc Natl Acad Sci U S A **86:**3867-3871.
35. **Goldberg MB, Theriot JA.** 1995. Shigella flexneri surface protein IcsA is sufficient to direct actin-based motility. Proc Natl Acad Sci U S A **92:**6572-6576.
36. **Burnaevskiy N, Fox TG, Plymire DA, Ertelt JM, Weigele BA, Selyunin AS, Way SS, Patrie SM, Alto NM.** 2013. Proteolytic elimination of N-myristoyl modifications by the Shigella virulence factor IpaJ. Nature **496:**106-109.

37. **Dobbs N, Burnaevskiy N, Chen D, Gonugunta VK, Alto NM, Yan N.** 2015. STING Activation by Translocation from the ER Is Associated with Infection and Autoinflammatory Disease. Cell Host Microbe **18:**157-168.

38. **Kentner D, Martano G, Callon M, Chiquet P, Brodmann M, Burton O, Wahlander A, Nanni P, Delmotte N, Grossmann J, Limenitakis J, Schlapbach R, Kiefer P, Vorholt JA, Hiller S, Bumann D.** 2014. Shigella reroutes host cell central metabolism to obtain high-flux nutrient supply for vigorous intracellular growth. Proc Natl Acad Sci U S A **111:**9929-9934.

39. **Lawhon SD, Maurer R, Suyemoto M, Altier C.** 2002. Intestinal short-chain fatty acids alter Salmonella typhimurium invasion gene expression and virulence through BarA/SirA. Mol Microbiol **46:**1451-1464.

40. **Huang Y, Suyemoto M, Garner CD, Cicconi KM, Altier C.** 2008. Formate acts as a diffusible signal to induce Salmonella invasion. J Bacteriol **190:**4233-4241.

41. **Yang F, Yang L, Chang Z, Chang L, Yang B.** 2018. Regulation of virulence and motility by acetate in enteropathogenic Escherichia coli. Int J Med Microbiol **308:**840-847.

42. **Datsenko KA, Wanner BL.** 2000. One-step inactivation of chromosomal genes in Escherichia coli K-12 using PCR products. Proc Natl Acad Sci U S A **97:**6640-6645.

43. **Murphy KC, Campellone KG.** 2003. Lambda Red-mediated recombinogenic engineering of enterohemorrhagic and enteropathogenic E. coli. BMC Mol Biol **4:**11.

44. **Li Y, Lin Z, Huang C, Zhang Y, Wang Z, Tang YJ, Chen T, Zhao X.** 2015. Metabolic engineering of Escherichia coli using CRISPR-Cas9 meditated genome editing. Metab Eng **31:**13-21.

45. **Tritt A, Eisen JA, Facciotti MT, Darling AE.** 2012. An integrated pipeline for de novo assembly of microbial genomes. PLoS One **7:**e42304.

46. **Duhl KL, Tefft NM, TerAvest MA.** 2018. Shewanella oneidensis MR-1 Utilizes both Sodium- and Proton-Pumping NADH Dehydrogenases during Aerobic Growth. Appl Environ Microbiol **84**.

Journal of Bacteriology

606 **Table 1.** Properties of the *Shigella flexneri* PE577 chromosome and plasmids

| | Length (bp) | % GC | Genes (Coding) | Pseudogenes | Accession No. |
|---|---|---|---|---|---|
| Chromosome | 4,591,632 | 51.0 | 3,897 | 662 | CP042980 |
| Plasmid 1 | 3,990 | 52.7 | 3 | 1 | CP042979 |
| Plasmid 2 | 3,128 | 45.1 | 7 | 1 | CP042978 |

607

608 **Table 2.** Pseudogenes unique to each strain. "Complete" implies a full-length gene, but potential
609 differences are based solely on genomic information and some genes may remain functional
610 even if truncated in length.

| Gene Name | Protein Name/Function | Complete in 2457T? | Complete in PE577? | Description/Comments |
|---|---|---|---|---|
| *acs* | acetate--CoA ligase | No | Yes | Truncation in CFS100 (248 aa); full length is 652 aa |
| *aes* | acetyl esterase | No | Yes | Truncation in CFS100 (272 aa); full length is 319 aa |
| *ag43* | autotransporter adhesin Ag43 | No | Yes | Truncation in CFS100 (297 aa); full length is 1040 aa |
| *arnA* | bifunctional UDP-4-amino-4-deoyl-L-arabinose formyltransferase/UDP glucuroncic acid oxidase | No | Yes | Truncation in CFS100 (258 aa); full length is 660 aa |
| *chbC* | PTS N,N'-diacetylchitobiose transporter subunit IIC | No | Yes | Truncation in CFS100 (63 aa); full length is 449 aa |
| *fusA* | elongation factor G | No | Yes | Truncation in CFS100 very early in protein (11 aa); full length is 704 aa |
| *glpD* | glycerol-3-phosphate dehydrogenase | No | Yes | Truncation in CFS100 (56 aa); full length is 501 aa |
| *glpF* | glycerol uptake facilitator protein GlpF | No | Yes | Truncation in CFS100 (214 aa); full length is 281 aa |
| *hexR* | DNA-binding transcriptional regulator HexR | No | Yes | Truncation in CFS100 (273 aa); full length is 289 aa |
| *mreC* | rod shape-determining protein MreC | No | Yes | Truncation in CFS100 (298 aa); full length is 367 aa |
| *nimT* | 2 nitroimidazole transporter | No | N/A | Completely absent in PE577 |
| *rpoS* | RNA polymeras sigma factor | No | Yes | Truncation in CFS100 (254 aa); full length is 330 aa |
| *tcyJ* | cystine ABC transporter substrate-binding protein | No | Yes | Truncation in CFS100 (176 aa); full length is 266 aa |
| *trbL* | P-type conjugative transfer protein | No | Yes | Truncation in CFS100 (261 aa); full length is 475 aa |
| *wcaC* | colonic acid biosynthesis glycosyltransferase | No | Yes | Truncation in CFS100 (202 aa); full length is 405 aa |
| *yfdV* | transporter YfdV | No | Yes | Truncation in CFS100 (253 aa); full length is 314 aa |
| *yijE* | cystine transporter YijE | No | Yes | Truncation in CFS100 (141 aa); full length is 301 aa |
| *acnA* | aconitate hydratase AcnA | Yes | No | Truncation in PE577 (237 aa); full length is 891 aa |
| *dmsA* | dimethylsulfoxide reductase subunit A | Yes | No | Truncation in PE577 (119 aa); full length is 814 aa |
| glcC | transcriptional regulator GlcC | Yes | Yes | Same sequence for residues 1-222; frameshift resulted in last 35 aa being different |
| *hycC* | formate hydrogenlyase subunit 3 | Yes | No | Truncation in PE577 (227 aa); full length is 500 aa |
| *malZ* | maltodextrin glucoside | Yes | No | Truncation in PE577 (391 aa); full length is 605 aa |
| *yrbL* | PhoP regulatory network protein YrbL | Yes | No | Truncation in PE577 (95 aa); full length is 210 aa |

611 **Figure 1.** Genome maps and features of the *S. flexneri* PE577 chromosome and plasmids, with
612 coding sequences (CDS), tRNA, rRNA, and GC characteristics colored as indicated. GC skew
613 refers to GC richness of a given region of the genome.

614

615 **Figure 2.** Growth of strains CFS100 and PE577 in nutrient-rich (LB) or nutrient-poor (M9)
616 media in aerobic conditions. Measurements are based on A) colony forming units per mL over
617 time or B) optical density at 600 nm. The relationship between these two measurements is
618 presented in C.

619

620 **Figure 3.** A) Pathways of pyruvate oxidation in *S. flexneri*. B) Comparison of genes involved in
621 the PoxB/Acs bypass or in formate detoxification between PE577 and CFS100. In the latter,
622 PoxB is grayed out because CFS100 encodes a truncated RpoS. Since RpoS controls *poxB*
623 expression, this may affect protein abundance. Similarly, FdhF is grayed out because it is a
624 pseudogene in both backgrounds but a different formate dehydrogenase may associate with the
625 FHL complex.

626

627 **Figure 4.** CFU/mL (A) and concentrations of formate (B), lactate (C), and acetate (D) in Δ*hycC*
628 strains with and without complementation after overnight growth. The strain is indicated on the
629 x-axis. Error bars represent standard error from three biological replicates.

630

631 **Figure 5.** CFU/mL (A) and concentrations of formate (B), lactate (C), and acetate (D) in strains
632 lacking various components of pyruvate oxidation pathways after overnight growth. The strain is
633 indicated on the x-axis. Error bars represent standard error from three biological replicates.

634

635

636

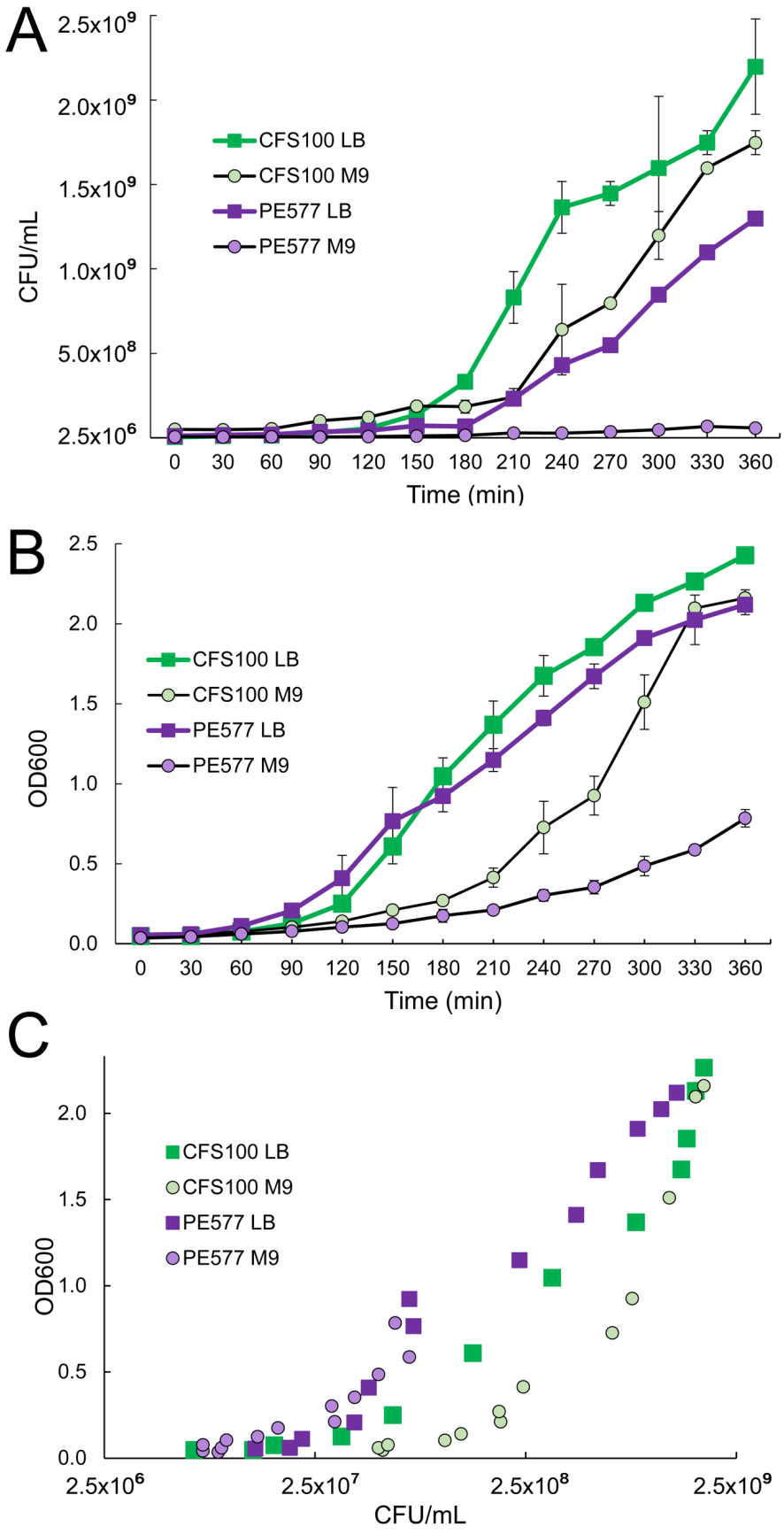

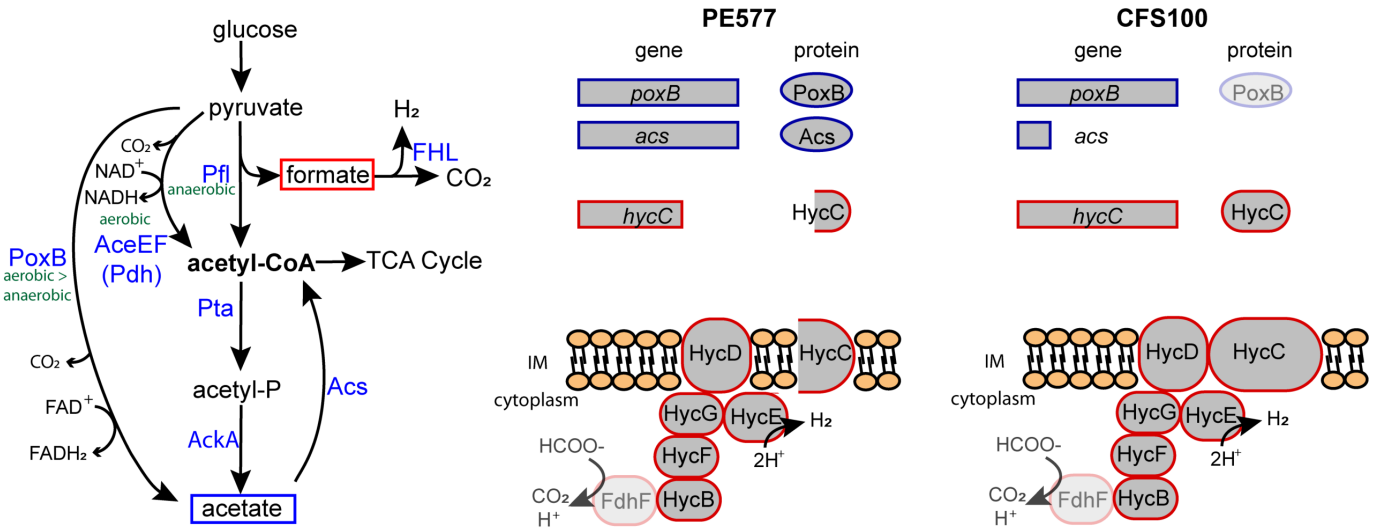

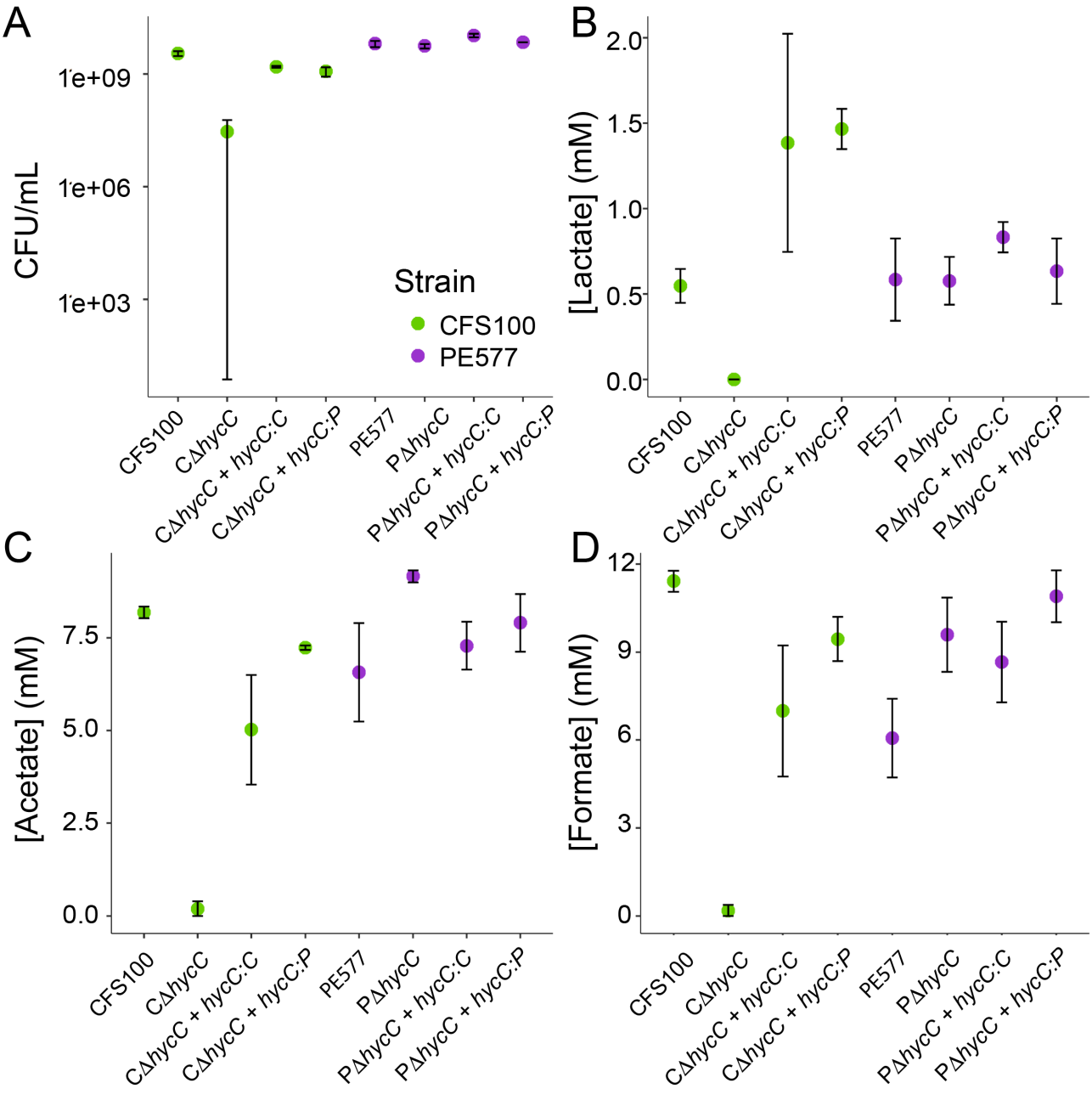

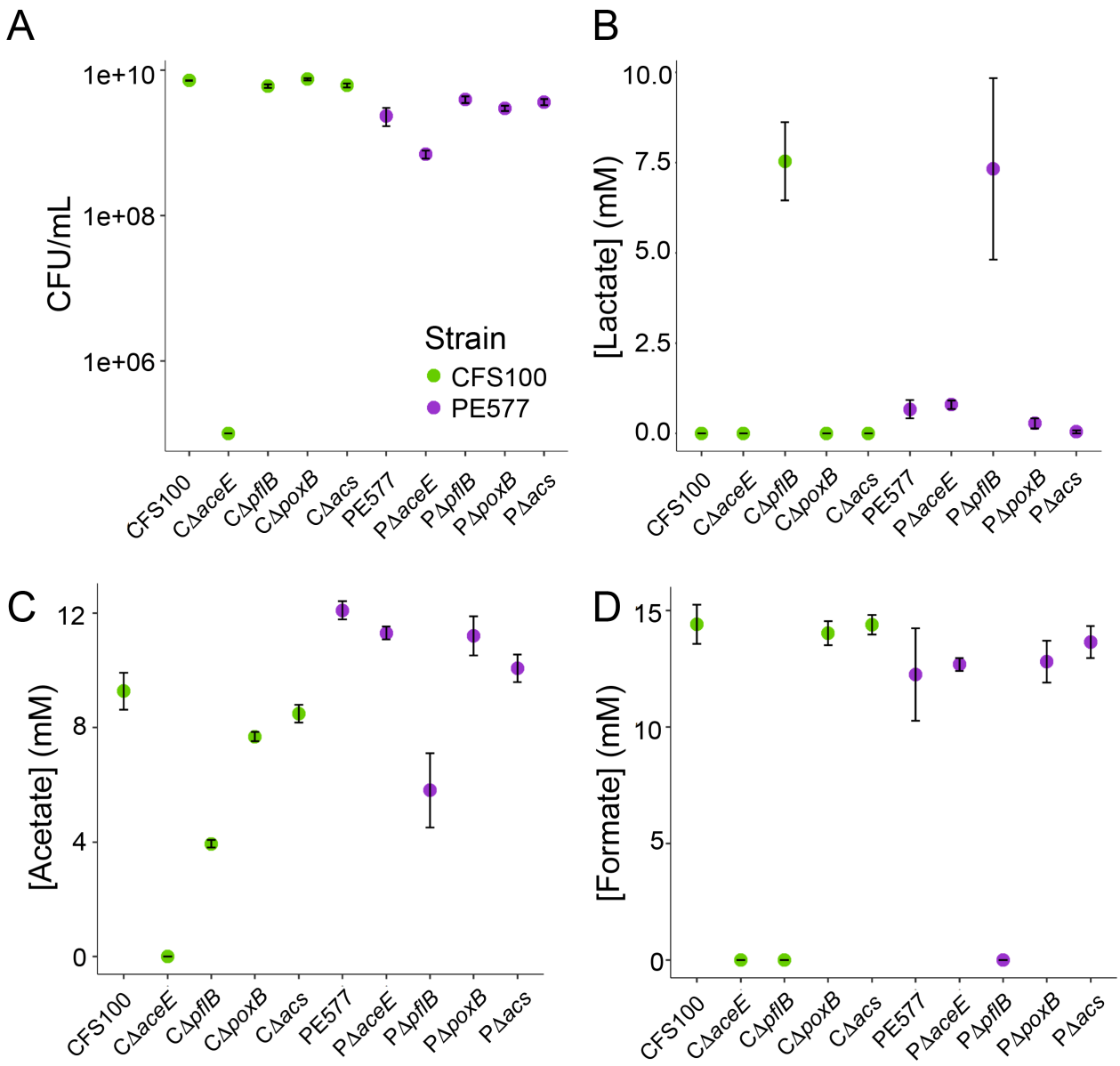

**Table 1.** Properties of the *Shigella flexneri* PE577 chromosome and plasmids

| | Length (bp) | % GC | Genes (Coding) | Pseudogenes | Accession No. |
|---|---|---|---|---|---|
| Chromosome | 4,591,632 | 51.0 | 3,897 | 662 | CP042980 |
| Plasmid 1 | 3,990 | 52.7 | 3 | 1 | CP042979 |
| Plasmid 2 | 3,128 | 45.1 | 7 | 1 | CP042978 |

**Table 2.** Pseudogenes unique to each strain. "Complete" implies a full-length gene, but potential differences are based solely on genomic information and some genes may remain functional even if truncated in length.

| Gene Name | Protein Name/Function | Complete in 2457T? | Complete in PE577? | Description/Comments |
|---|---|---|---|---|
| *acs* | acetate--CoA ligase | No | Yes | Truncation in CFS100 (248 aa); full length is 652 aa |
| *aes* | acetyl esterase | No | Yes | Truncation in CFS100 (272 aa); full length is 319 aa |
| *ag43* | autotransporter adhesin Ag43 | No | Yes | Truncation in CFS100 (297 aa); full length is 1040 aa |
| *arnA* | bifunctional UDP-4-amino-4-deoyl-L-arabinose formyltransferase/UDP glucuroncic acid oxidase | No | Yes | Truncation in CFS100 (258 aa); full length is 660 aa |
| *chbC* | PTS N,N'-diacetylchitobiose transporter subunit IIC | No | Yes | Truncation in CFS100 (63 aa); full length is 449 aa |
| f*usA* | elongation factor G | No | Yes | Truncation in CFS100 very early in protein (11 aa); full length is 704 aa |
| *glpD* | glycerol-3-phosphate dehydrogenase | No | Yes | Truncation in CFS100 (56 aa); full length is 501 aa |
| *glpF* | glycerol uptake facilitator protein GlpF | No | Yes | Truncation in CFS100 (214 aa); full length is 281 aa |
| *hexR* | DNA-binding transcriptional regulator HexR | No | Yes | Truncation in CFS100 (273 aa); full length is 289 aa |
| *mreC* | rod shape-determining protein MreC | No | Yes | Truncation in CFS100 (298 aa); full length is 367 aa |
| *nimT* | 2 nitroimidazole transporter | No | N/A | Completely absent in PE577 |
| *rpoS* | RNA polymeras sigma factor | No | Yes | Truncation in CFS100 (254 aa); full length is 330 aa |
| *tcyJ* | cystine ABC transporter substrate-binding protein | No | Yes | Truncation in CFS100 (176 aa); full length is 266 aa |
| *trbL* | P-type conjugative transfer protein | No | Yes | Truncation in CFS100 (261 aa); full length is 475 aa |
| *wcaC* | colonic acid biosynthesis glycosyltransferase | No | Yes | Truncation in CFS100 (202 aa); full length is 405 aa |
| *yfdV* | transporter YfdV | No | Yes | Truncation in CFS100 (253 aa); full length is 314 aa |
| *yijE* | cystine transporter YijE | No | Yes | Truncation in CFS100 (141 aa); full length is 301 aa |
| *acnA* | aconitate hydratase AcnA | Yes | No | Truncation in PE577 (237 aa); full length is 891 aa |
| *dmsA* | dimethylsulfoxide reductase subunit A | Yes | No | Truncation in PE577 (119 aa); full length is 814 aa |
| glcC | transcriptional regulator GlcC | Yes | Yes | Same sequence for residues 1-222; frameshift resulted in last 35 aa being different |
| *hycC* | formate hydrogenlyase subunit 3 | Yes | No | Truncation in PE577 (227 aa); full length is 500 aa |
| *malZ* | maltodextrin glucoside | Yes | No | Truncation in PE577 (391 aa); full length is 605 aa |
| *yrbL* | PhoP regulatory network protein YrbL | Yes | No | Truncation in PE577 (95 aa); full length is 210 aa |